

Simulations of weld pool dynamics in V-groove GTA and GMA welding

Dae-Won Cho · Suck-Joo Na · Min-Hyun Cho · Jong-Sub Lee

Received: 20 September 2011 / Accepted: 20 August 2012
© International Institute of Welding 2013

Abstract

Introduction Many simulation models use an axisymmetric arc model for heat flux, arc pressure, and electromagnetic force. In V-groove welding, however, an elliptically symmetric arc model is more acceptable than an axisymmetric model. An elliptically symmetric arc model can be established by applying the Abel inversion method to CCD images of welding arc on V-groove.

Methods This study uses an elliptically symmetric arc model for CFD based simulations of fluid flow behavior in weld pool of GMA V-groove welding. It recommends a new method of calculating the electromagnetic force distribution in V-groove welding.

Conclusion A volume of fluid method is used to describe the molten pool flow in numerical simulations.

Keywords (IIW Thesaurus) Arc welding · Electromagnetic fields · Simulating

1 Introduction

Many pipe welding experiments and simulations have been conducted in V-groove or fillet joint for the purpose of analyzing and optimizing the welding parameters [1, 2]. However, optimizing the parameters in gas metal arc (GMA) welding is complicated by the force of gravity, which causes a molten pool to flow to the ground. Because of the need to check the molten pool flow, a computational fluid dynamics (CFD)

model is consequently more suitable than a normal finite elements method model.

Many V-groove joint simulations use an axisymmetric arc heat flux model [3, 4]. However, they generally ignore the effect of the joint shape, which can change the arc plasma characteristics. Cho obtained an arc heat distribution in a V-groove gas tungsten arc welding (GTAW) with several arc images from of CCD camera; also obtained the area matrix Abel inversion method and found out that the arc heat distribution appeared to be elliptically symmetric [5]. An elliptically symmetric arc shape in V-groove welding affects several important models that contain an effective radius of arc plasma. Examples include an arc heat flux model, an arc pressure model and an electromagnetic force (EMF) model. The application of an elliptically symmetric arc heat flux model or an arc pressure in V-groove welding is relatively easy because both models are used for the boundary conditions on the upper surface of a workpiece. However, the EMF is more complicated in CFD based simulations of weld pool behavior: the body force appears to affect both the boundary and inner areas of the molten region. Additionally, Fig. 1 shows that the concept of current flow pattern in V-groove welding is very different from the bead on plate (BOP) welding. Without a consideration of the current flow pattern in V-groove welding, the molten pool flow from the EMF model may not be described realistically.

For the more realistic simulation results, this study suggests a new method of applying the coordinate mapping in V-groove welding and assumes the arc model as an elliptically symmetric shape.

2 Numerical formulations

2.1 Governing equations

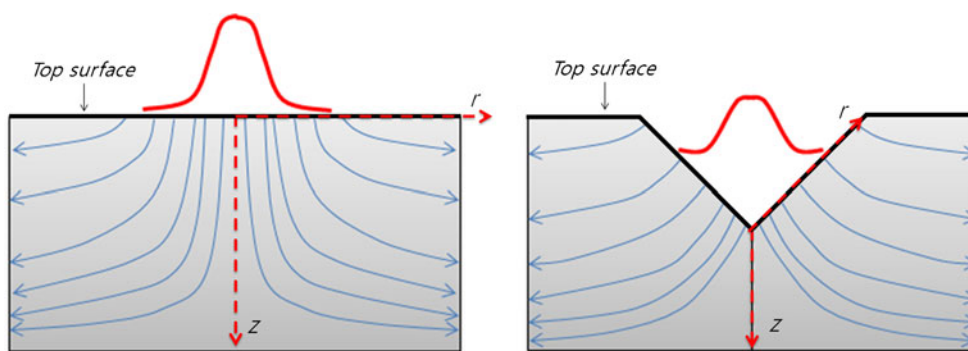
The governing equations in CFD simulations of a weld pool include a continuity equation, a momentum equation and an

Doc. IIW-2312, recommended for publication by Commission XII
“Arc Welding Processes and Production Systems”

D.-W. Cho · S.-J. Na (✉)
Department of Mechanical Engineering, KAIST, Daejeon,
Republic of Korea
e-mail: sjoona@kaist.ac.kr

M.-H. Cho · J.-S. Lee
Technical Research Laboratories, POSCO, Pohang,
Republic of Korea

Fig. 1 The concept of current flow patterns in BOP and V-groove welding



energy equation. The first two equations are called, the Navier–Stokes equations. The commercial package Flow-3D was used for the simulation with a VOF equations. [6–8]. The material properties and variables are summarized in Table 1.

2.2 Boundary conditions

The energy on the top free surface is balanced among the arc heat flux (Q_A), the heat dissipation by convection (Q_{conv}) and radiation (Q_{rad}) and heat loss due to evaporation (Q_{evap}). The energy balance on the top surface is expressed as the following equations:

$$k \frac{\partial T}{\partial n} = Q_A - Q_{conv} - Q_{rad} - Q_{evap}. \quad (1)$$

In V-groove welding, the elliptically symmetric model is better to use for an arc heat flux [2]. Thus, this study uses an elliptically symmetric which is based on the two different effective radii ($\sigma_x=1.50$ mm, $\sigma_y=0.90$ mm) of the arc

plasma in Eq. (2). This equation contains the average value of voltage (V), current (I) from the welding experiments and the arc efficiency in GMAW and GTAW.

$$Q_A(x, y) = \frac{\eta_{Arc_GTAW} VI}{2\pi\sigma_x\sigma_y} \exp\left(-\left(\frac{x^2}{2\sigma_x^2}\right) - \left(\frac{y^2}{2\sigma_y^2}\right)\right) \quad (2)$$

$$Q_A(x, y) = \frac{\eta_{Arc_GMAW} VI}{2\pi\sigma_x\sigma_y} \exp\left(-\left(\frac{x^2}{2\sigma_x^2}\right) - \left(\frac{y^2}{2\sigma_y^2}\right)\right)$$

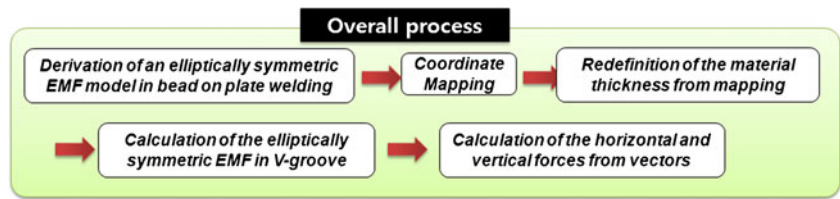
This study adopted the arc efficiency (η_{Arc_GTAW}) in GTAW as 0.7 because many previous studies already used the value in GTAW [9, 10]. On the other hand, the efficiency of the arc in GMAW is predetermined as 0.56 because the heat input efficiency of the droplets was found to be 0.24 from Eqs (3), (4), (5), and (6). Normally, the total GMAW efficiency was set at 0.8 [7, 9].

$$f_d = \frac{3r_w^2 WFR}{4r_d^3}, \quad (3)$$

Table 1 Prosperities used in simulation

Symbol	Nomenclature	Symbol	Nomenclature
k	Thermal conductivity	μ_m	Material permeability, 1.26×10^6 H/m
\vec{n}	Normal vector to free surface	q_d	Heat input from droplet
η_{Arc_GTAW}	Arc efficiency in GTAW, 0.7	ρ	Density, (solid:7.8, liquid:6.9, g/cm ³)
η_{Arc_GMAW}	Arc efficiency in GMAW, 0.56	C_s	Specific heat of solid, 7.26×10^6 erg/gsK
V	Welding voltage (average)	C_l	Specific heat of liquid, 7.32×10^6 erg/gsK
I	Welding current (average)	T_s	Solidus temperature, 1768 K
J	Current density (I/mm ²)	T_l	Liquidus temperature, 1798 K
σ_x	Effective radius of arc in x-direction, 1.5 mm	T_o	Room temperature, 298 K
σ_y	Effective radius of arc in y-direction, 0.90 mm	h_{sl}	Latent heat of fusion, 2.77×10^9 erg/gs
f_d	Droplet frequency (Hz)	η_d	Droplet efficiency in GMAW, 0.24
WFR	Wire feed rate (m/min)	z	Vertical distance from top surface
r_w	Wire diameter in GMAW, 1.2 mm	J_{ze}	Vertical component of the current density
r_d	Droplet diameter in GMAW, 1.2 mm	J_{re}	Radial component of the current density
μ_0	Permeability of vacuum, 1.26×10^6 H/m	$B_{\theta e}$	Angular component of the magnetic field
γ	Surface tension		

Fig. 2 The process of elliptically symmetric EMF calculation in V-groove welding



$$q_d = \frac{4}{3} \pi r_d^3 \rho [C_s(T_s - T_o) + C_l(T_d - T_s) + h_{sl}] f_d, \quad (4)$$

$$\eta_d = \frac{q_d}{VI}, \quad (5)$$

$$\eta_{Arc_GMAW} = 0.8 - \eta_d. \quad (6)$$

The energy balance on the bottom free surface is expressed in a manner similar to Eq. (1) but the arc heat flux model should be eliminated. For the pressure boundary conditions, the following Eq. (7) is used at the free surface.

$$p = p_A + \frac{\gamma}{R_c}, \quad (7)$$

$$p_A = \frac{\mu_0 I J}{4\pi}, \quad (8)$$

$$p_A(x, y) = \frac{\mu_0 I^2}{4\pi^2 \sigma_x \sigma_y} \exp\left(-\left(\frac{x^2}{2\sigma_x^2}\right) - \left(\frac{y^2}{2\sigma_y^2}\right)\right), \quad (9)$$

In Eq. (8), the current density (J) is assumed to be linearly proportional to the arc pressure (p_A) [11]. Thus, the distribution of the arc pressure follows the distribution of the current density. The arc plasma pressure can therefore be modeled, as shown in Eq. (9) with an elliptically symmetric model that has the same effective radii of arc heat flux [2].

2.3 EMF model

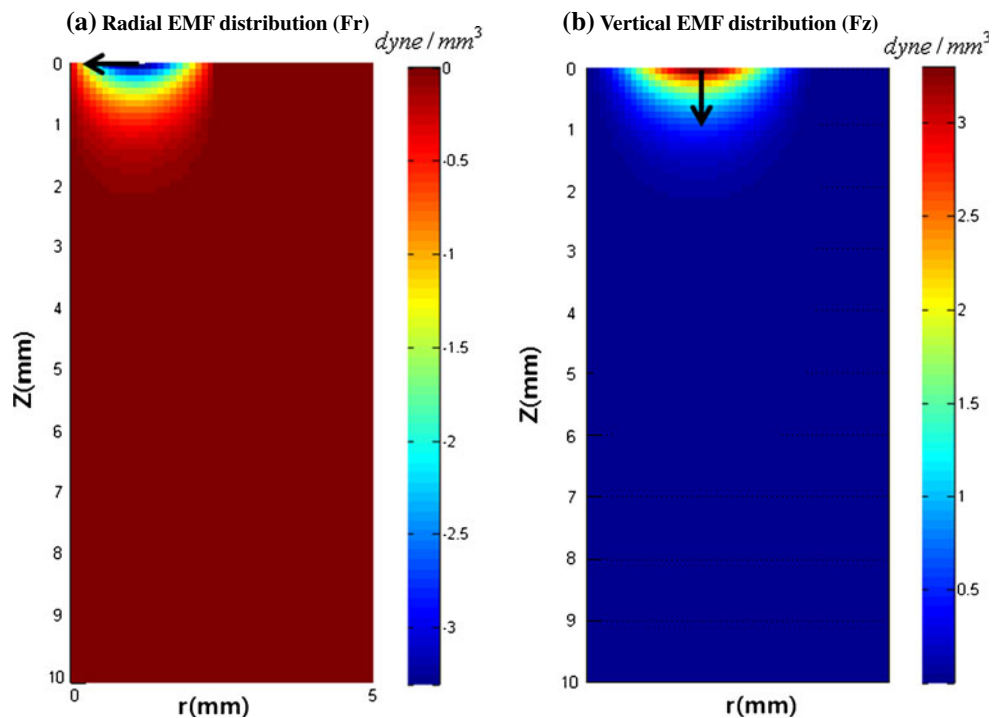
Figure 2 shows several procedures that must be conducted for the implementation of the elliptically symmetric EMF model of the commercial software Flow-3D.

2.3.1 Derivation of an elliptically symmetric EMF model in bead-on-plate welding

In BOP welding, the welding current is released from the top surface as a Gaussian distribution. Therefore, as shown in Fig. 3, the axisymmetric radial and vertical EMF distributions [6] can be applied to welding simulations. Additionally, most of the EMF distributions are clearly concentrated on the top surface.

The axisymmetric EMF model must be modified because the arc heat flux model is elliptically symmetric in V-groove

Fig. 3 Radial and vertical of the axisymmetric EMF distributions. **a** Radial EMF distribution (F_r). **b** Vertical EMF distribution (F_z)



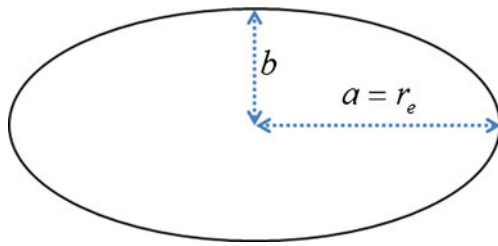


Fig. 4 Elliptic shape and elliptic radius (r_e)

welding. Equations (10), (11), and (12) can be used to formulate Eq. (13), which is a simple elliptically symmetric model that contains an effective radius of welding arc for the x-direction as well as the elliptic radius (r_e) in Fig. 4. This model modifies the current density and electromagnetic field and ultimately determines the EMF for the x, y, and z directions (F_x, F_y, F_z).

$$\frac{x^2}{a^2} + \frac{y^2}{b^2} = 1, \quad (10)$$

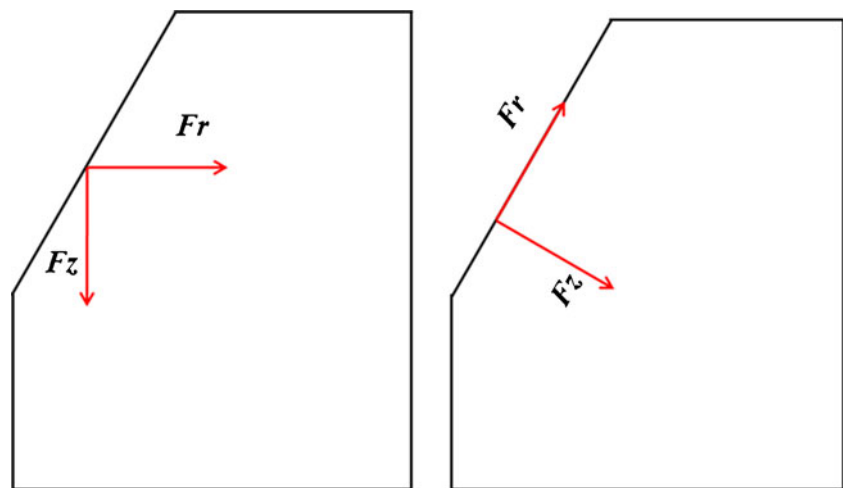
$$k_1 = \frac{b}{a} = \frac{\sigma_y}{\sigma_x}, \quad (11)$$

$$x^2 + \frac{y^2}{k_1^2} = r_e^2, \quad (12)$$

$$\exp\left(-\frac{x^2}{2\sigma_x^2} - \frac{y^2}{2\sigma_y^2}\right) = \exp\left(-\frac{r_e^2}{2\sigma_x^2}\right), \quad (13)$$

$$J_{ze} = \frac{I}{2\pi} \int_0^\infty \lambda J_0(\lambda r_e) \exp(-\lambda^2 \sigma_x^2 / 4d) \frac{\sinh[\lambda(c_y - z)]}{\sinh(\lambda c_y)} d\lambda, \quad (14)$$

Fig. 5 Radial and vertical EMF directions on the slope surface. **a** EMF directions of Cartesian coordinate. **b** Ideal EMF directions



(a) EMF directions of Cartesian coordinate

(b) Ideal EMF directions

$$J_{re} = \frac{I}{2\pi} \int_0^\infty \lambda J_1(\lambda r_e) \exp(-\lambda^2 \sigma_x^2 / 4d) \frac{\cosh[\lambda(c_y - z)]}{\sinh(\lambda c_y)} d\lambda, \quad (15)$$

$$B_{\theta e} = \frac{\mu_m I}{2\pi} \int_0^\infty J_1(\lambda r_e) \exp(-\lambda^2 \sigma_x^2 / 4d) \frac{\sinh[\lambda(c_y - z)]}{\sinh(\lambda c_y)} d\lambda, \quad (16)$$

$$F_x = -J_{ze} B_{\theta e} \frac{x}{r_e}, \quad (17)$$

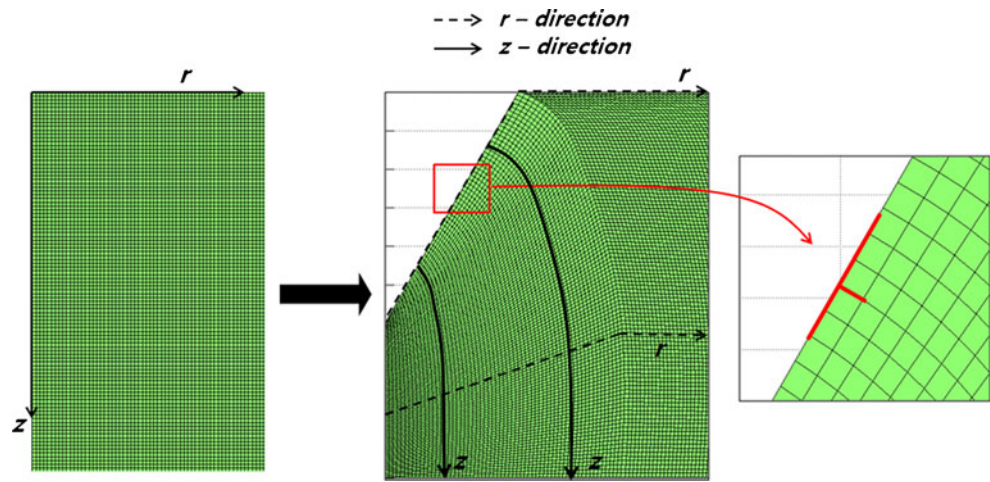
$$F_y = -J_{ze} B_{\theta e} \frac{y}{r_e}, \quad (18)$$

$$F_z = J_{ze} B_{\theta e}. \quad (19)$$

2.3.2 Coordinate mapping

Mapping is used to calculate the EMF in V-groove welding. The radial and vertical direction of the EMF is the same as the r -direction and z -direction in BOP welding. However, both directions of the EMF must be different from each other on the V-groove slope surface because, as shown in Fig. 5 the welding current starts to flow into the workpiece through the top surface.

Fig. 6 Result of coordinate mapping



2.3.3 Mapping the coordinates for the V-groove welding

The new coordinates can be generated with the following mapping steps:

(a) The V-groove slope surface is assumed to be a top surface.

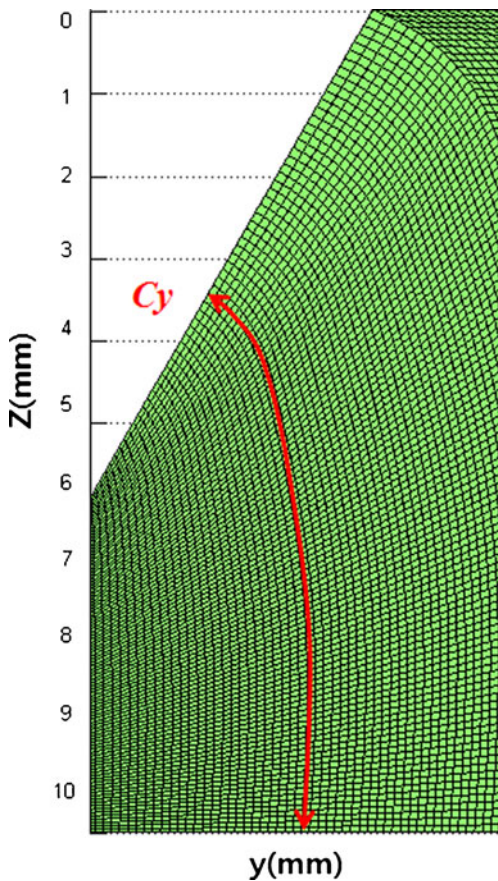


Fig. 7 Redefinition of material thickness (C_y)

- (b) The current density starts to flow perpendicular to the V-groove slope surface.
- (c) The use of a spline function forms, the coordinates inside the workpiece.

Therefore, as shown in Fig. 6, the new coordinates could be derived from the process of coordinate mapping.

2.3.4 Redefinition of the material thickness from mapping

The mapping coordinates confirm that the thickness of the V-groove joint is crucial for determining the EMF value: however, as shown in Fig. 7, the thickness is changed along the r -direction as shown in Fig. 7. The newly calculated thickness (C_y) is applied to the EMF models in Eqs. (14), (15), and (16).

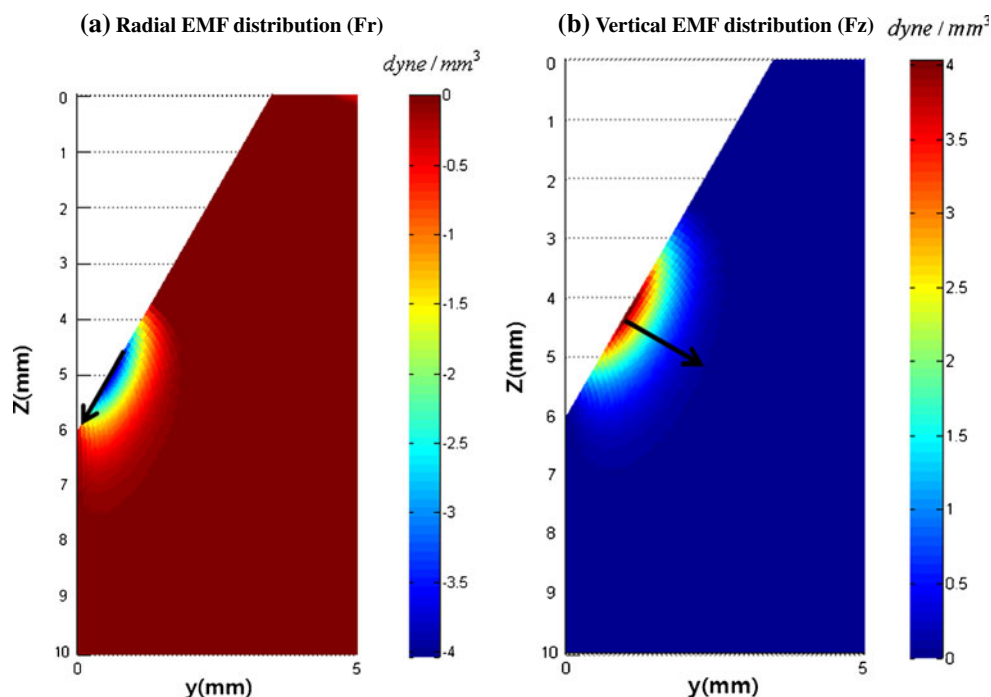
2.3.5 Calculation of the elliptically symmetric EMF in V-groove joint

Figure 8 shows the calculation of the EMF distributions for the radial and vertical directions in V-groove. The values used in the calculations are the values presented in Sections 2.3.1 to 2.3.4. However, these directions are unsuitable for use in an isotropic Cartesian coordinate system and were consequently modified with the corresponding vectors.

2.3.6 Calculation of the horizontal and vertical forces from vectors

EMF in V-groove GTAW The coordinate mapping enables the EMF vectors to be determined from the neighboring coordinates. As shown in Fig. 9, the locations of points $P1$, $P2$, and $P3$ can be automatically determine the two neighboring angles θ_1 and θ_2 . Figure 10 shows that it is then

Fig. 8 EMF distributions in V-groove. Radial EMF distribution (F_r) Vertical EMF distribution (F_z)



possible to obtain the EMF from Eqs. (20) and (21) for the vertical and horizontal directions (F_{y1} , F_{z1}). In Fig. 8, the locations of the maximum absolute EMF value for the radial and vertical components are different from each other; therefore, the horizontal EMF component has two opposite directions in Fig. 10. If no additional deposit metal is deposited on the surface, this method is acceptable for use in simulations of GTAW processes.

$$F_{y1} = F_z \cos(\theta_1) + F_r \cos(\theta_2) \quad (20)$$

$$F_{z1} = F_z \sin(\theta_1) - F_r \sin(\theta_2) \quad (21)$$

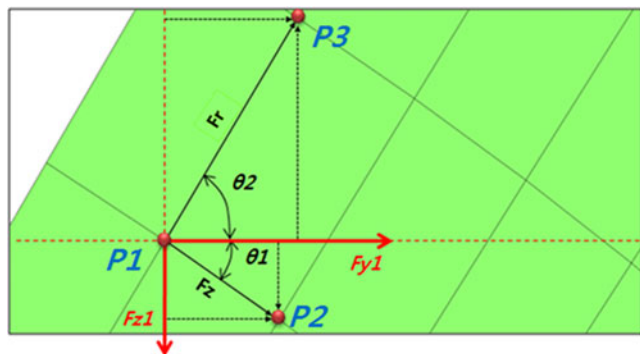


Fig. 9 EMF vectors

When the material melts by arc heat, the molten pool surface cannot maintain the inclined flat surface as before. Thus, this study detects the deformed molten pool free surface and redistributes the EMF values (S_{ij}) by considering the free surface location of z -direction as shown in Fig. 11. Therefore, the coordinate of EMF from mapping move upward or downward along the z -direction. Finally, the newly defined EMF values are applied in the simulation.

EMF in V-groove GMAW In GTAW, hardly any of the tungsten electrodes melts, so the electrode deposits almost no molten metal. In GMAW, on the other hand, molten droplets from electrode wire impinge on the weld pool and tend to accumulated. As shown in Fig. 12, GMAW produces a surface that has more of a flat bead shape than the inclined shape of a V-groove joint. Figure 13 shows that if the molten pool surface is flat in V-groove GMAW, the deposit metal area and the mapping coordinates can be described in terms of the wire feed rate and welding speed. The elliptically symmetric models and coordinate mapping in Fig. 14a show that most of the EMF distributions are focused near the flat surface of the molten pool region. Moreover, if the top surface of the deposit metal is flat, the coordinate system under the top surface is the same with Cartesian coordinate system as shown in Fig. 13. Therefore, the results of EMF distributions, before and after the coordinate mapping, are almost the same each other; thus, the coordinate mapping process is not required in GMAW simulations. The same

Fig. 10 EMF distributions with vectors. Horizontal EMF distribution Vertical EMF distribution

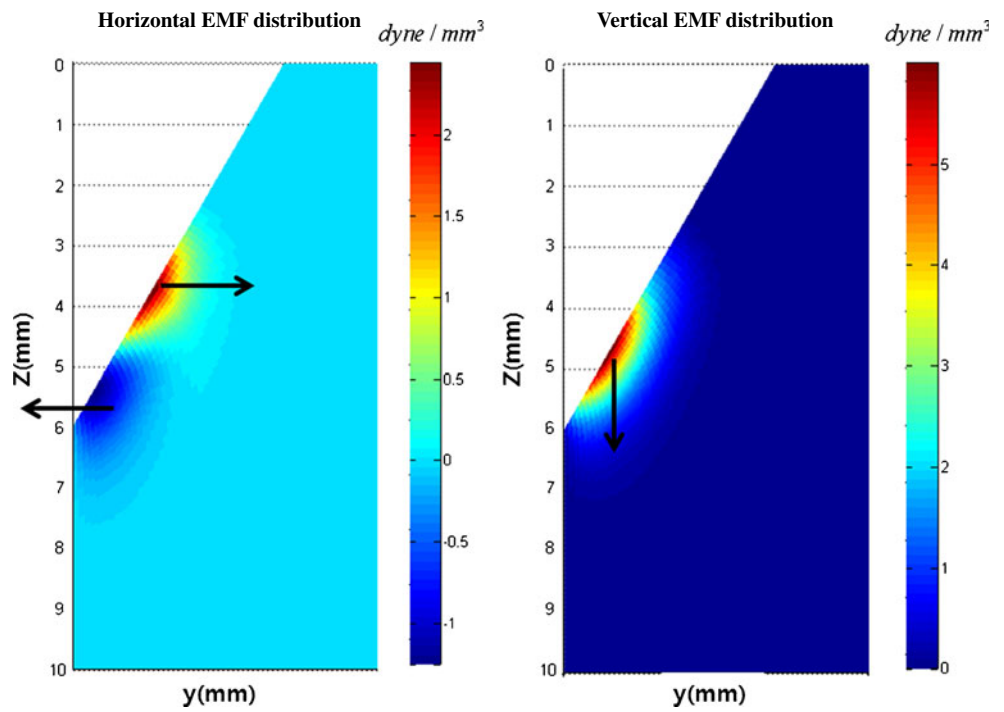


Fig. 11 The V-groove surface deformation in GTAW. **a** Before melting. **b** After melting

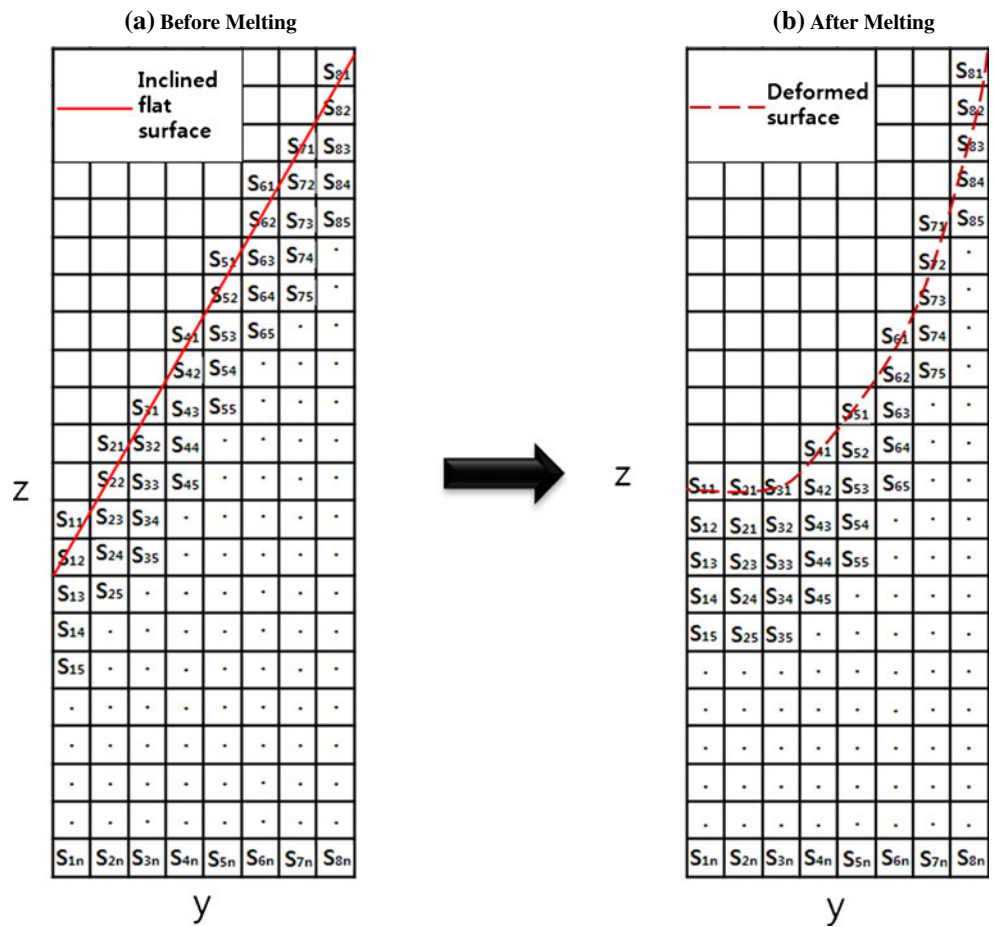
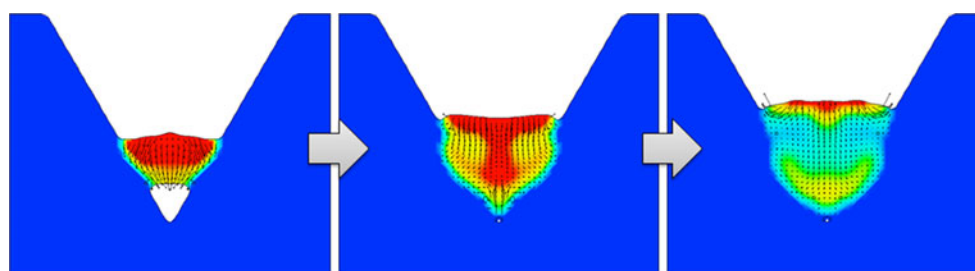


Fig. 12 Flat molten pool surfaces in GMAW



way with GTAW, the newly defined EMF values in GMAW by considering the deformed free surface are applied in the simulation.

2.4 Other welding models

In some welding models of a welding arc, such as the buoyancy force and drag force of arc plasma, the effective radius of the welding arc is sometimes ignored. However, this study relies on the same axisymmetric models that were used for these terms in other studies [6–8].

3 Result and discussion

3.1 Simulation results of GTAW in coordinate mapping of the EMF

Another model that does not use coordinate mapping was used to validate the coordinate mapping of the EMF. In that model, the EMF vectors that head to the center and bottom surface produce a counter-clockwise molten pool flow; as shown in Fig. 15a, this type of flow produces deep penetration and leads to the formation of a narrow bead. When coordinate mapping is used, the radial EMF vectors have two opposite directions inward and outward; furthermore, as shown in Fig. 10, the vertical EMF vector head exclusively to the bottom surface. The inner radial EMF vector can be

balanced by the surface tension and drag force, as shown in Fig. 15b, produce a tiny inward molten pool flow. In contrast, the outward EMF vector can be strengthened by the surface tension and drag force, which cause a clockwise molten pool flow; thus, in the numerical simulation, the bead is wide, the penetration is shallow, and the reinforcement is high. Figure 16 shows that the result from the simulation with the coordinate mapping of the EMF in GTAW is in a good agreement with the experimental results. The parameters used in GTAW experiments are listed in Table 2.

3.2 Simulation results of GMAW from an elliptically symmetric EMF

Figure 17 shows that because the coordinate mapping of the EMF is not required in V-groove GMAW, the elliptically symmetric EMF model can be used directly in simulations. In Fig. 18, the final bead shape obtained from the simulation appears to be very similar to the bead shape in the experiment. These results confirm the validity of the elliptically symmetric EMF model. The parameters used in GMAW experiments are listed in Table 3.

4 Conclusions

In V-groove welding, the arc is rather elliptically symmetric than axisymmetric. An elliptically symmetric arc model is

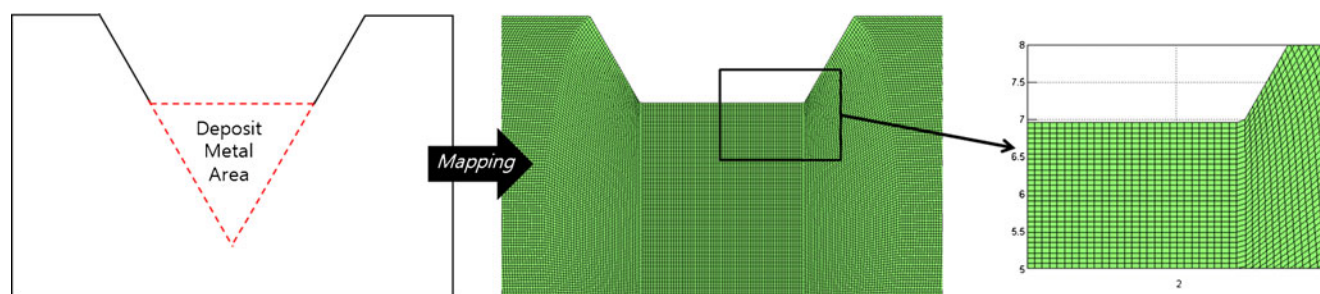
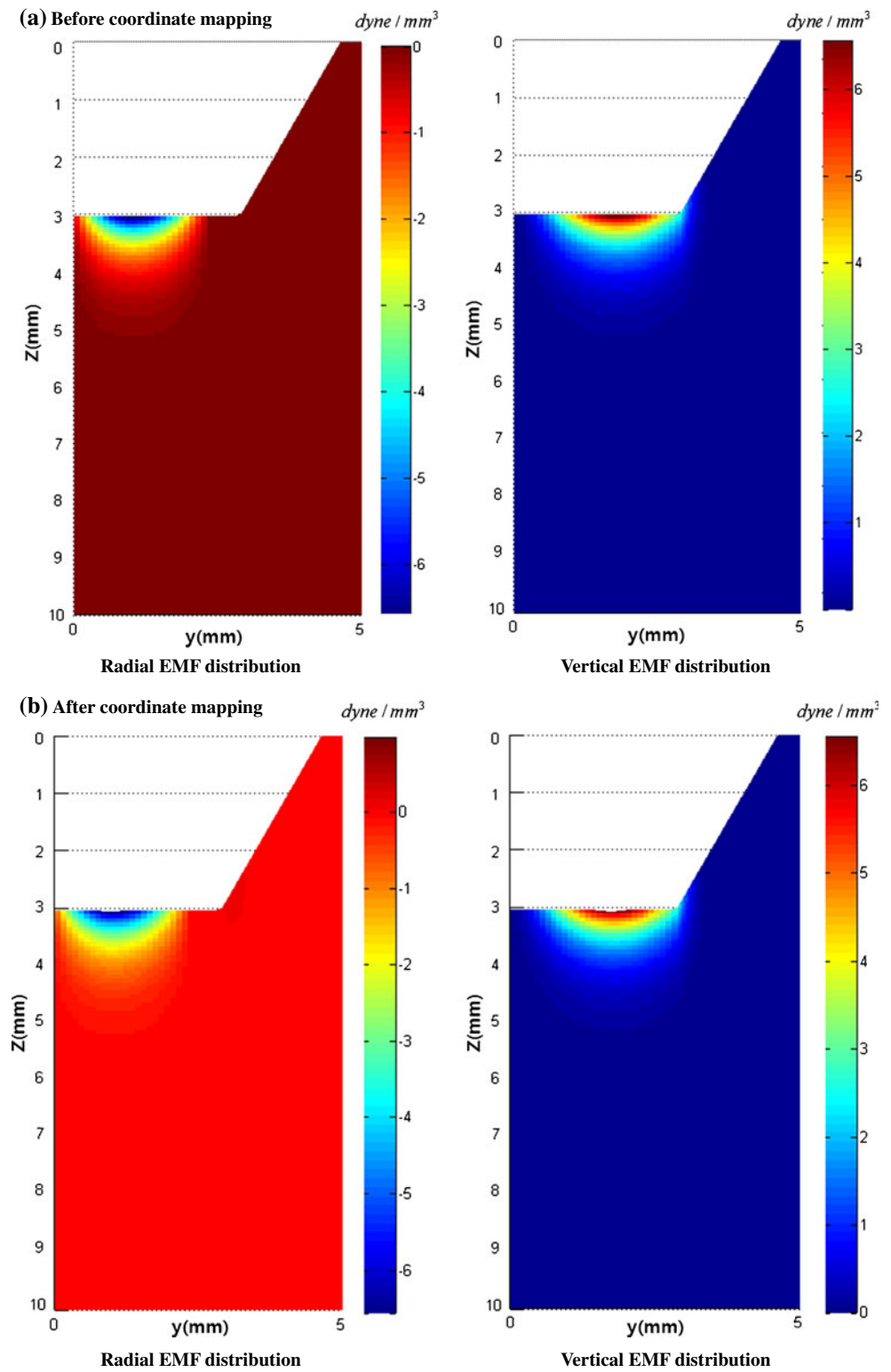


Fig. 13 Coordinates mapping in V-groove GMAW. (WFR: 7.5 m/min, current: 255A, welding speed: 10 mm/s, ϕ 1.2 mm)

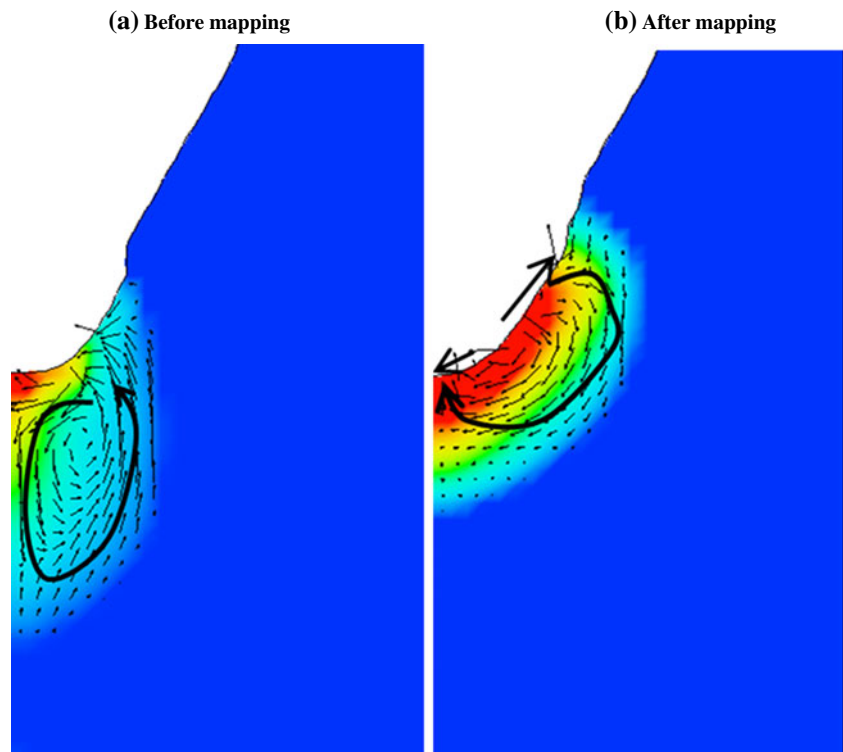
Fig. 14 EMF distributions in GMAW. Radial EMF distribution. Vertical EMF distribution. **a** Before coordinate mapping. Radial EMF distribution. Vertical EMF distribution. **b** After coordinate mapping



therefore useful for the arc heat flux, the arc pressure and the EMF distribution. An arc heat flux and an arc pressure

model can be used in boundary conditions; however, the EMF model can be used for the body force, which affects

Fig. 15 Molten pool flow pattern in GTAW. **a** Before mapping. **b** After mapping



the entire molten pool volume. In V-groove GMAW, the top surface of the molten pool is almost flat; thus, coordinate mapping is not strictly required in CFD-based process simulations. In contrast with GMAW, however, the top surface of the molten pool in GTAW is inclined because there is no additional volume to form the bead shape. This paper suggests and validates a new method that can effectively model

Table 2 Welding parameters in GTAW

Current	Voltage	Arc length	Welding speed	Electrode
200A	12.6 V	5 mm	stationary	Tungsten, ϕ 2.4 mm

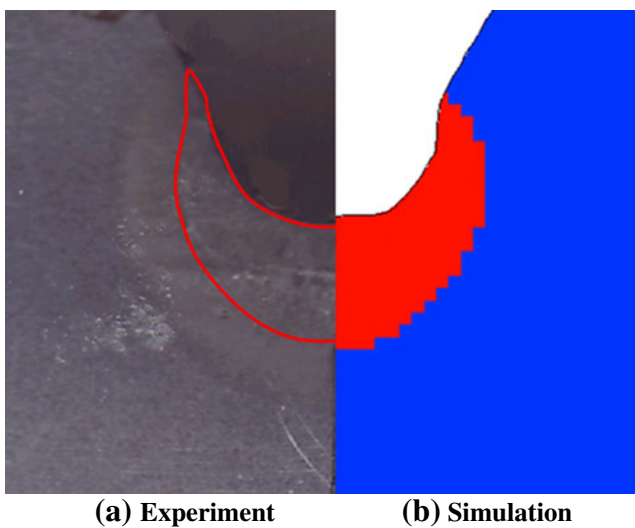


Fig. 16 Comparison experiment with simulation in GTAW. **a** Experiment. **b** Simulation

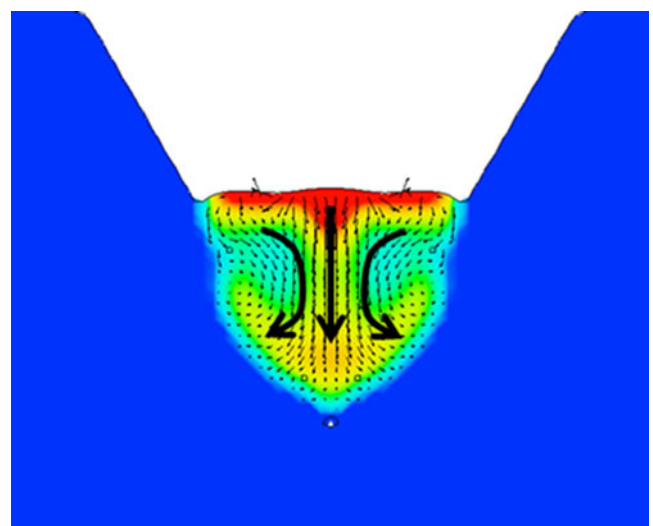


Fig. 17 Molten pool flow pattern in GMAW

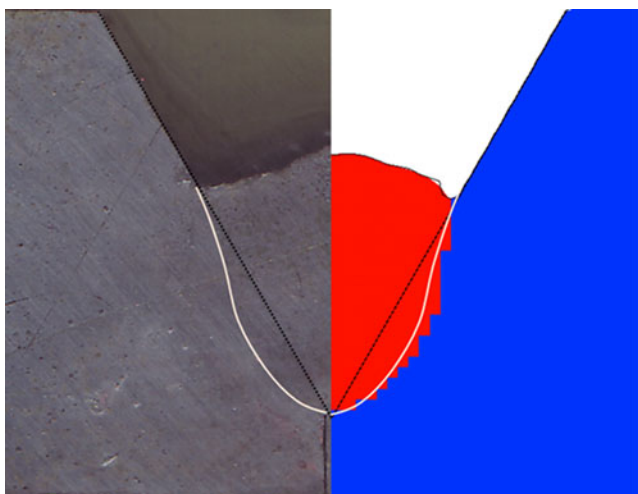


Fig. 18 Comparison of simulation with experiment in GMAW

the EMF in V-groove GTAW; in the new method, coordinate mapping is applied to CFD-based simulations of weld pool fluid dynamics.

Table 3 Welding parameters in GMAW

Current	Voltage	CTWD	Welding speed	Electrode	Shielding gas
255A (WFR:7.5 m/min)	25 V	20 mm	10 mm/s	YGW15, ϕ 1.2 mm	Ar80% CO ₂ 20 %, 20 l/min

Acknowledgements The authors gratefully acknowledge the support by Brain Korea 21 Project and POSCO in Republic of Korea.

References

1. Cho DW, Na SJ, Lee MY (2009) Expectation of bead shape using non-linear multiple regression and piecewise cubic hermite interpolation in FCA fillet pipe welding. *J KWJS* 27(5):42–48, in Korean
2. Cho DW, Na SJ, Cho MH, Lee MY (2011) A study on molten pool flow for various welding positions of V-groove GMA pipe welding. IITW conference, Istanbul
3. Zhang W, Kim CH, DebRoy T (2004) Heat and fluid flow in complex joints during gas metal arc welding part II. *J Appl Phys* 95(9):5220–5229
4. Hu J, Tsai HL (2008) Modeling of transport phenomena in 3D GMAW of thick metals with V groove. *J Phys D Appl Phys* 41(6):065202
5. Cho YT, Na SJ (2005) Application of Abel inversion in real-time calculations for circularly and elliptically symmetric radiation sources. *Meas Sci Technol* 16(3):878–884
6. Cho WI, Na SJ, Cho MH, Lee JS (2010) Numerical study of alloying element distribution in CO₂ laser–GMA hybrid welding. *Comput Mater Sci* 49(4):792–800
7. Cho JH, Na SJ (2009) Three-dimensional analysis of molten pool in GMA-laser hybrid welding. *Weld J* 88(2):35s–43s
8. Cho MH, Lim YC, Farson DF (2006) Simulation of weld pool dynamics in the stationary pulsed gas metal arc welding process and final weld shape. *Weld J* 85(12):271s–283s
9. Dupont JN, Marder AR (1995) Thermal efficiency of arc welding processes. *Weld J* 74(12):406s–416s
10. Reddy AA, Guha B, Achar DRG (2002) Finite Element modeling of three-dimensional transient heat transfer in stainless steel (304) pulsed GTA weldments. *Numer Heat Tran Part A* 41(1):41–46
11. Lin ML, Eagar TW (1986) Pressures produced by gas tungsten arcs. *Metall Mater Trans B* 17(3):601–607